Compressive beamforming

Angeliki Xenaki[a)] and Peter Gerstoft
Scripps Institution of Oceanography, University of California San Diego, La Jolla, California 92093-0238

Klaus Mosegaard
Department of Applied Mathematics and Computer Science, Technical University of Denmark, Kongens Lyngby, 2800 Denmark

Sound source localization with sensor arrays involves the estimation of the direction-of-arrival (DOA) from a limited number of observations. Compressive sensing (CS) solves such underdetermined problems achieving sparsity, thus improved resolution, and can be solved efficiently with convex optimization. The DOA estimation problem is formulated in the CS framework and it is shown that CS has superior performance compared to traditional DOA estimation methods especially under challenging scenarios such as coherent arrivals and single-snapshot data. An offset and resolution analysis is performed to indicate the limitations of CS. It is shown that the limitations are related to the beampattern, thus can be predicted. The high-resolution capabilities and the robustness of CS are demonstrated on experimental array data from ocean acoustic measurements for source tracking with single-snapshot data. © 2014 Acoustical Society of America.
[http://dx.doi.org/10.1121/1.4883360]

I. INTRODUCTION

The problem of direction-of-arrival (DOA) estimation with sensor arrays, encountered in electromagnetic, acoustic and seismic imaging, is to infer the number and the location of (usually few) sources possibly in the presence of noise from measurements of the wavefield with an array of sensors. Conventional beamforming[1] is the simplest traditional method for DOA estimation, though it is characterized by low resolution. Other methods[2] developed to overcome the resolution limit of conventional beamforming have degraded performance under noisy conditions, coherent sources and few snapshots.

The compressive sensing (CS) framework asserts that the underlying *sparse* signals can be reconstructed from very few measurements by solving a convex minimization problem. Exploiting the inherent sparsity of the underlying signal, CS outperforms traditional methods which aim to minimize the energy of the reconstructed signal resulting in low-resolution, non-sparse solutions. The convex formulation of CS offers computational efficiency compared to other sparsity promoting methods.

CS (Refs. 3 and 4) has found applications in a wide range of scientific fields from medical[5,6] and ultrasound imaging,[7] to error correction in channel coding,[8] radar detection,[9] seismic imaging[10,11] and image reconstruction[12] to name a few. In ocean acoustics, CS is shown to improve the performance of matched field processing,[13] which is a generalized beamforming method for localizing sources in complex environments, and of coherent passive fathometry in inferring the number and depth of sediment layer interfaces.[14]

Indications of the super-resolution (i.e., finer resolution than conventional beamforming) and robustness of CS in DOA estimation are also presented in Refs. 15 and 16. Malioutov *et al.*[15] study the performance of CS in DOA estimation with respect to noise, source number and coherence. Edelmann and Gaumond[16] compare CS with conventional beamforming using towed array data and show that the CS has superior performance, which is more pronounced with undersampling.

We demonstrate the robustness of CS in sound source localization with sensor arrays, especially with coherent arrivals, single-snapshot data and random array geometries. A systematic analysis of offset and resolution is introduced. It is shown that the limitations of the method depend on the array geometry, the frequency, the location of the actual sources and the relative noise level and that they can be predicted from the beampattern.

Moreover, we investigate an iterative reweighed optimization process[17–19] for more accurate localization combined with a level-correction post-processing step to significantly improve the reconstruction. The superiority of CS in terms of accurate localization, improved resolution and artifact reduction is demonstrated on source tracking from experimental single-snapshot data from ocean acoustic measurements.

In the following, vectors are represented by bold lower-case letters and matrices by bold uppercase letters. The transpose and Hermitian (i.e., conjugate transpose) operators are denoted by T and H, respectively. The l_p-norm of a vector $\mathbf{x} \in \mathbb{C}^n$ is defined as $\|\mathbf{x}\|_p = \left(\sum_{i=1}^{n} |x_i|^p\right)^{1/p}$. By extension, the l_0-norm is defined as $\|\mathbf{x}\|_0 = \sum_{i=1}^{n} 1_{x_i \neq 0}$.

II. SPARSE RECONSTRUCTION WITH COMPRESSIVE SENSING

Many engineering problems involve either the reconstruction of a signal of interest or the estimation of its

[a)]Author to whom correspondence should be addressed. Current address: Department of Applied Mathematics and Computer Science, Technical University of Denmark, Kongens Lyngby, 2800 Denmark. Electronic mail: anxe@dtu.dk

0001-4966/2014/136(1)/260/12/$30.00   © 2014 Acoustical Society of America

parameters from a (usually small) number of observations. Compressive sensing, also known as compressed sensing[20] or compressive sampling,[21] is a method for solving such underdetermined problems assuring very accurate reconstruction under two conditions:[3,21,22]

(1) sparsity of the underlying signal,
(2) sufficient incoherence of the process which maps the underlying signal to the observations.

A concise description of the method follows.

Let $\mathbf{x} \in \mathbb{C}^N$ be an unknown vector representing the underlying signal we aim to reconstruct. The signal $\mathbf{x}$ is sparse, i.e., it has only K nonzero elements with $K \ll N$. An example of such a sparse signal is the frequency domain representation of a sinusoidal time signal. Let $\mathbf{y} \in \mathbb{C}^M$ be a vector of measurements linearly related to the signal $\mathbf{x}$, e.g., time samples of the sinusoidal signal. In the absence of noise, the vectors $\mathbf{x}$ and $\mathbf{y}$ are related by a linear set of equations, $\mathbf{y} = \mathbf{A}\mathbf{x}$. The sensing matrix $\mathbf{A} = \mathbf{\Psi\Phi}$ is the product of the matrix $\mathbf{\Phi}_{N \times N}$, which transforms the signal from one domain to another [e.g., the inverse discrete Fourier transform (IDFT) for a time-frequency representation], and the matrix $\mathbf{\Psi}_{M \times N}$, which represents the measurement process (e.g., time sampling).

The matrix $\mathbf{A}$ is assumed known and fixed (it does not adapt to the information on the signal $\mathbf{x}$). In the case that $M < N$, the problem is underdetermined and does not have a unique solution. A way of solving this ill-posed problem is constraining the possible solutions with prior information, here by exploiting sparsity.

By definition, sparsity can be imposed on $\mathbf{x}$ by minimizing the l_0-norm, which counts the number of non-zero entries in the vector, leading to the minimization problem (P_0),

$$\min_{\mathbf{x} \in \mathbb{C}^N} \|\mathbf{x}\|_0 \text{ subject to } \mathbf{y} = \mathbf{A}\mathbf{x}. \qquad (P_0)$$

However, the minimization problem (P_0) is a nonconvex combinatorial problem which becomes computationally intractable even for moderate dimensions. The breakthrough of CS came with the proof that for sufficiently sparse signals and sensing matrices with sufficiently incoherent columns[23,24] the (P_0) problem is equivalent to the (P_1) problem,[5,20,25]

$$\min_{\mathbf{x} \in \mathbb{C}^N} \|\mathbf{x}\|_1 \text{ subject to } \mathbf{y} = \mathbf{A}\mathbf{x}. \qquad (P_1)$$

The l_1 relaxation (P_1) of the (P_0) problem (also known as basis pursuit[26]) is the closest convex optimization problem to (P_0) and can be solved efficiently even for large dimensions. Moreover, due to the convexity of the l_1-norm, the method of minimizing (P_1) converges to the global minimum. Other l_p-norm relaxations of the (P_0) problem for $0 < p < 1$, which also favor sparsity, are nonconvex and convergence to global minima is not guaranteed.[17,27]

For comparison, traditional methods solve the underdetermined problem $\mathbf{y} = \mathbf{A}_{M \times N}\mathbf{x}$, $M < N$ by seeking the solution with the minimum l_2-norm through the minimization problem (P_2),

$$\min_{\mathbf{x} \in \mathbb{C}^N} \|\mathbf{x}\|_2 \text{ subject to } \mathbf{y} = \mathbf{A}\mathbf{x}. \qquad (P_2)$$

The problem (P_2) is convex and has the analytic minimum length solution,

$$\hat{\mathbf{x}} = \mathbf{A}^H (\mathbf{A}\mathbf{A}^H)^{-1} \mathbf{y}. \qquad (1)$$

It aims to minimize the energy of the signal through the l_2-norm, rather than its sparsity, hence its solution is non-sparse. Thus, the problem (P_1) has increased performance over (P_2) for sparse signals (at the cost of computational complexity since it does not have an analytic solution) and it can be solved efficiently with convex optimization.

Figure 1 depicts the geometry of the l_p-norm minimization problem, for $p = 0, 1, 2$ constrained to fit the data. To keep the visualization intuitive, an example is considered where the sparse vector $\mathbf{x} \in \mathbb{R}^2$, with a single nonzero element ($\|\mathbf{x}\|_0 = 1$), is to be recovered by $\mathbf{y} \in \mathbb{R}$ linear measurements. Since there are less measurements than unknowns, all $\mathbf{x}$ residing on the line $\mathbf{y} = \mathbf{A}\mathbf{x}$ satisfy the constraint. A unique solution is found only by providing additional information about $\mathbf{x}$. For example, we seek the one with the minimum l_p-norm [by solving either (P_0), (P_1), (P_2)].

Geometrically, all vectors with l_p-norm less or equal to a value $r \in \mathbb{R}$ are on an l_p-ball with radius r, $\{\mathbf{x}| \ \|\mathbf{x}\|_\mathbf{p} \leq r\}$. In $\mathbb{R}^2$, the l_2-ball is a disk while the l_1-ball is a rhombus. The solution $\mathbf{x}$ is the intersection of the measurement line and the smallest l_p-ball. The l_2-norm optimization problem, Fig. 1(c), results almost always in non-sparse solutions due to the curvature of the l_2-ball. In contrast, the edginess of the l_1-ball favors sparse solutions, Fig. 1(b), and likely leads to the solution of the l_0-norm problem, Fig. 1(a).

The theory extends to noisy measurements and compressible signals (approximately sparse)[28] making the framework useful for practical applications. Assuming that the measurements are contaminated with additive noise $\mathbf{n} \in \mathbb{C}^M$ such that $\mathbf{y} = \mathbf{A}\mathbf{x} + \mathbf{n}$ the (P_1) problem is reformulated as
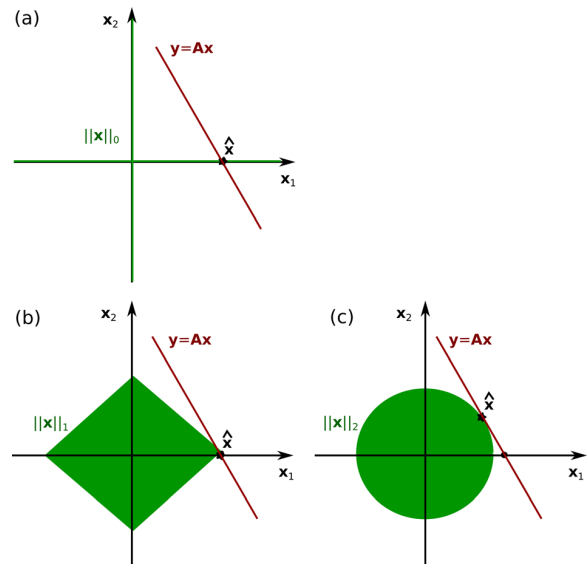

FIG. 1. (Color online) Geometric visualization of (a) the l_0-norm, (b) the l_1-norm, and (c) the l_2-norm problem in $\mathbb{R}^2$. The solution $\hat{\mathbf{x}}$ is the intersection of the measurement line $\mathbf{y} = \mathbf{A}\mathbf{x}$ and the minimum norm-ball in each case.

$$\min_{\mathbf{x} \in \mathbb{C}^N} \|\mathbf{x}\|_1 \text{ subject to } \|\mathbf{Ax} - \mathbf{y}\|_2 \leq \epsilon, \qquad (P_1^\epsilon)$$

where ϵ is an upper bound for the noise norm, such that $\|\mathbf{n}\|_2 \leq \epsilon$. The solution to (P_1^ϵ) has the minimum l_1-norm while it fits the data up to the noise level. (P_1^ϵ) can be reformulated in an unconstrained form with the use of Lagrange multipliers,

$$\min_{\mathbf{x} \in \mathbb{C}^N} \|\mathbf{Ax} - \mathbf{y}\|_2^2 + \eta\|\mathbf{x}\|_1. \qquad (P_1^\eta)$$

The regularization parameter η controls the relative importance between the sparsity of the solution (l_1-norm term) and the fit to the measurements (l_2-norm term).

Herein, we use the cvx toolbox for disciplined convex optimization which is available in the MATLAB environment. It uses interior point solvers to obtain the global solution of a well-defined optimization problem.[29–31]

III. COMPRESSIVE SENSING FOR DOA ESTIMATION

In this section, we apply the CS for DOA estimation and compare it with widely used localization methods, namely, conventional (delay-and-sum) beamforming (CBF), minimum variance distortionless response (MVDR) beamforming, and the multiple signal classification (MUSIC) method.[2,32] The focus is on obtaining the accurate locations of the sources rather than their amplitudes since the amplitudes can be adjusted in a further step after the locations are recovered (see Sec. V).

In the following, the sound speed and the geometry of the array are assumed known. We further assume that the sources are in the farfield of the array (i.e., plane waves), the processing is narrowband and the problem is confined in two dimensions (2D) with a linear array of sensors and the sources residing in the plane of the array. These assumptions only serve simplicity. CS, as the other localization methods, is universal and can be extended to three-dimensions (3D) and arrays with arbitrary (but known) geometry, as random arrays.

The location of a source is characterized by the direction of arrival of the associated plane wave $\theta \in [-90°, 90°]$ with respect to the array axis. The propagation delay from the ith potential source to each of the array sensors is described by the steering (or replica) vector,

$$\mathbf{a}(\theta_i) = \frac{1}{\sqrt{M}} e^{j(2\pi/\lambda)\mathbf{r}\sin\theta_i}, \qquad (2)$$

where λ is the wavelength and $\mathbf{r} = [r_1, ..., r_M]^T$ comprises the sensor locations. The normalization $1/\sqrt{M}$, such that $\|\mathbf{a}\|_2 = 1$, is to simplify the analysis.

To infer the unknown number and locations, θ, of the sources, the problem of DOA estimation is formulated as a spatial spectrum estimation problem where the source locations are estimated from the received signal $\mathbf{y}$.

Let the unknown vector $\mathbf{x} \in \mathbb{C}^N$ comprise the source amplitudes at all directions $\theta \in [-90°, 90°]$ on the grid of interest. Let $\mathbf{y} \in \mathbb{C}^M$ be the vector of wavefield

measurements at the M sensors. Practically, we are interested in a fine resolution on the angular grid, thus $M < N$. The sensing matrix is formed by the steering vectors at all potential source directions as its columns,

$$\mathbf{A}_{M \times N} = [\mathbf{a}(\theta_1), ..., \mathbf{a}(\theta_N)]. \qquad (3)$$

It is the product of a matrix, $\mathbf{\Psi}$, representing the spatial sampling of the wavefield at the sensor locations and an IDFT basis, $\mathbf{\Phi}$, connecting the dimensionless spatial domain of the sensor locations *per* wavelength, $\mathbf{r}/\lambda$, and the DOA domain in terms of $\sin\theta$.

In the presence of additive noise $\mathbf{n} \in \mathbb{C}^M$, the measurement vector is described by

$$\mathbf{y} = \mathbf{Ax} + \mathbf{n}. \qquad (4)$$

In the following, the noise is generated as independent and identically distributed complex Gaussian. The array signal-to-noise ratio (SNR) for a single snapshot is used, defined as $\text{SNR} = 20\log_{10}(\|\mathbf{Ax}\|_2/\|\mathbf{n}\|_2)$. The choice of the array SNR, which determines the noise l_2-norm $\|\mathbf{n}\|_2 = \|\mathbf{Ax}\|_2 10^{-\text{SNR}/20}$, serves the analytic study of the (P_1^ϵ) problem.

A. CBF

The CBF (Ref. 1) is the simplest source localization method. The method combines the sensor outputs coherently to enhance the signal at a specific look direction from the ubiquitous noise, yielding the estimate

$$\hat{\mathbf{x}} = \mathbf{A}^H \mathbf{y}. \qquad (5)$$

It can be seen as a solution, Eq. (1), to the l_2-norm minimization problem (P_2) with the simplifying assumption $\mathbf{AA}^H = \mathbf{I}_M$. The CBF is robust to noise but suffers from low resolution and the presence of sidelobes. The spatial resolution at each look direction, θ_i, $i = 1, ..., N$, is indicated by the beampattern, $|\mathbf{A}^H\mathbf{a}(\theta_i)|$, i.e., the ith column of $|\mathbf{A}^H\mathbf{A}|$ ($|\cdot|$ is the elementwise absolute value).

The CBF power spectrum is

$$P_{\text{CBF}}(\theta) = \mathbf{a}(\theta)^H \hat{\mathbf{R}}_\mathbf{y} \mathbf{a}(\theta), \qquad (6)$$

where $\hat{\mathbf{R}}_\mathbf{y} = (1/L)\sum_{l=1}^{L} \mathbf{y}_l \mathbf{y}_l^H$ is the cross-spectral matrix from L snapshots (i.e., observations of $\mathbf{y}$ at a particular frequency). CBF is robust to noise and can be used even with single snapshot data ($L = 1$) but suffers from low resolution and the presence of sidelobes.

B. MVDR beamformer

The MVDR weight vector[33] is obtained by minimizing the output power of the beamformer under the constraint that the signal from the look direction, θ, remains undistorted,

$$\min_{\mathbf{w}} \mathbf{w}^H \hat{\mathbf{R}}_\mathbf{y} \mathbf{w} \text{ subject to } \mathbf{w}^H \mathbf{a}(\theta) = 1, \qquad (7)$$

resulting in the optimal weight vector

$$\mathbf{w}_{\text{MVDR}}(\theta) = \frac{\hat{\mathbf{R}}_{\mathbf{y}}^{-1}\mathbf{a}(\theta)}{\mathbf{a}(\theta)^H \hat{\mathbf{R}}_{\mathbf{y}}^{-1}\mathbf{a}(\theta)}. \tag{8}$$

The regularized inverse $(\hat{\mathbf{R}}_{\mathbf{y}} + \beta\mathbf{I}_M)^{-1}$ with regularization parameter β is used instead of $\hat{\mathbf{R}}_{\mathbf{y}}^{-1}$, whenever the cross-spectral matrix is rank deficient. The MVDR beamformer power spectrum is

$$P_{\text{MVDR}}(\theta) = \mathbf{w}_{\text{MVDR}}(\theta)^H \hat{\mathbf{R}}_{\mathbf{y}} \mathbf{w}_{\text{MVDR}}(\theta). \tag{9}$$

C. MUSIC

MUSIC (Ref. 34) is based on the eigendecomposition of the cross-spectral matrix and the separation of the signal and the noise subspaces,

$$\hat{\mathbf{R}}_{\mathbf{y}} = \hat{\mathbf{U}}_s \hat{\mathbf{\Lambda}}_s \hat{\mathbf{U}}_s^H + \hat{\mathbf{U}}_n \hat{\mathbf{\Lambda}}_n \hat{\mathbf{U}}_n^H. \tag{10}$$

The signal eigenvectors, $\hat{\mathbf{U}}_s$, corresponding to the largest eigenvalues, $\hat{\mathbf{\Lambda}}_s$, are in the same subspace as the steering vectors, Eq. (2), while the noise eigenvectors, $\hat{\mathbf{U}}_n$, are orthogonal to the subspace of the steering vectors thus $\mathbf{a}(\theta)^H\hat{\mathbf{U}}_n = \mathbf{0}$.

MUSIC uses the orthogonality between the signal and the noise subspaces to locate the maxima in the spectrum,

$$P_{\text{MUSIC}}(\theta) = \frac{1}{\mathbf{a}(\theta)^H\hat{\mathbf{U}}_n\hat{\mathbf{U}}_n^H\mathbf{a}(\theta)}. \tag{11}$$

Both MVDR and MUSIC overcome the resolution limit of the conventional beamformer by exploiting signal information conveyed by the cross-spectral matrix. However, their performance depends on the eigenvalues of the cross-spectral matrix thus it degrades with few snapshots, when the cross-spectral matrix is rank deficient, and in the presence of coherent sources, when the signal subspace is reduced (Chap. 9 in Ref. 32). CS does not have these limitations as it utilizes directly the measured pressure $\mathbf{y}$.

D. Compressive sensing

Usually, there are only few sources $K \ll N$ present and a sparse solution $\mathbf{x}$ can be obtained which honors the data, Eq. (4), using the l_1-norm for sparsity and the l_2-norm for noise (P_1^ϵ).

CS for DOA estimation as the solution to the problem (P_1^ϵ) is formulated for a single snapshot. Figure 2(a) compares CBF and CS in the case of a single snapshot. Given a good choice of ϵ, that is $\epsilon = \|\mathbf{n}\|_2$ for the single snapshot case, CS locates the two sources correctly while CBF cannot resolve them as separate due to their proximity. The CS resolution limitations in relation to the SNR and the choice of ϵ are discussed in Secs. IV F and V, respectively.

To compare CS with other methods which involve the cross-spectral matrix, we formulate the method under the multiple snapshots scenario. For L snapshots, the measurement matrix is $\mathbf{Y} = \mathbf{AX} + \mathbf{N}$, where $\mathbf{Y}$ and $\mathbf{N}$ are $M \times L$ matrices and $\mathbf{X}$ has dimensions $N \times L$.

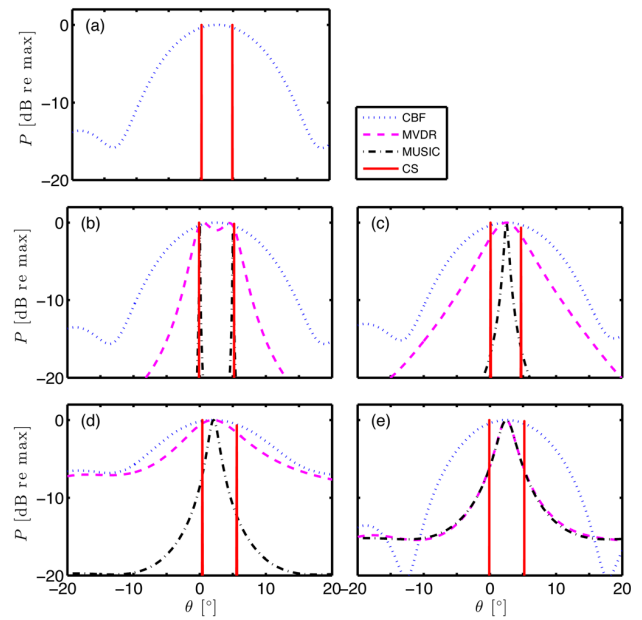For moving sources, it befits to solve one optimization problem for each snapshot sequentially, resulting in a sparse

FIG. 2. (Color online) DOA estimation from L snapshots for two equal-strength sources at $0°$ and $5°$ with a uniform linear array with $M = 8$ sensors and spacing $d/\lambda = 1/2$. (a) CBF and CS for uncorrelated sources with SNR $= 20$ dB and one snapshot, $L = 1$. CBF, MVDR, MUSIC, and CS for uncorrelated sources with (b) SNR $= 20$ dB and $L = 50$, (c) SNR $= 20$ dB and $L = 4$, (d) SNR $= 0$ dB and $L = 50$, and (e) for correlated sources with SNR $= 20$ dB and $L = 50$. The array SNR is for one snapshot.

solution for each snapshot.[35] For stationary sources, a way to combine the multiple snapshots is by minimizing the l_1-norm of the vector $\mathbf{x}_{l_2}$ resulting from calculating the l_2-norm of the row vectors in $\mathbf{X}$ (see Ref. 15 for details),

$$\min\|\mathbf{x}_{l_2}\|_1 \text{ subject to } \|\mathbf{AX} - \mathbf{Y}\|_2 \le \epsilon. \tag{12}$$

Figures 2(b)–2(e) compare the CBF, MVDR, MUSIC, and CS methods for DOA estimation. The noise bound, ϵ, is used both as a regularization parameter for the regularized inverse of the cross-spectral matrix in the case of snapshot-starved data, i.e., $L < M$, in MVDR and as a separation limit between the signal and noise subspace eigenvalues in MUSIC.

CBF fails to discern the two closely spaced sources. MVDR and MUSIC provide high resolution under high array SNR and uncorrelated sources but their performance degrades significantly under snapshot-starved data, correlated sources, and noisy conditions. CS resolves the two sources with high resolution in all cases and indicates the applicability of the method in detection of coherent arrivals (such as multipath arrivals) and when a limited number of snapshots is available.

In the following, the CS formulation for a single snapshot is used except at the end of Sec. VI.

IV. LIMITATIONS

CS offers super-resolution due to the sparsity constraint imposed by the minimization of the l_1-norm of the signal. However, as all DOA estimation methods, it also has limitations. In this section, we analyze the performance of CS in DOA estimation in terms of the discretization of the angular space, the coherence of the sensing matrix and the SNR.

A. Basis mismatch

The fundamental assumption in CS is the sparsity of the underlying signal in the basis of representation, $\mathbf{A}$. However, a mismatch between the assumed and the actual basis may cause the signal to appear as incompressible. One such example is the mismatch of a DFT basis in FFT beamforming due to inadequate discretization of the DOA domain. When the sources do not coincide with the points on the selected angular grid (particularly in the case of moving sources), the signal might not appear sparse in the selected DFT basis due to spatial spectral leakage. Since the fundamental assumption of sparsity is violated, the CS reconstruction might have poor performance under basis mismatch. An analysis of the sensitivity of CS to basis mismatch is found in Ref. 36.

Herein, we assume that the problem is discretized densely enough to avoid basis mismatch and we study the limitations of CS due to a coherent basis.

B. Coherent or redundant basis

To guarantee good performance of the CS in parameter estimation, the columns of the sensing matrix should be incoherent, i.e., sufficiently uncorrelated.[28] In this case, the optimization problems (P_0) and (P_1) are equivalent, resulting in the same unique solution.

Random matrices with Gaussian independent and identically distributed entries are ideal sensing matrices in CS due to their very low coherence.[8,20] Monajemi et al.[37] extend the utility of CS to cases which involve some types of deterministic sensing matrices.

Many problems involve sensing matrices with highly coherent columns. A common example is when $\mathbf{A}$ is an oversampled DFT basis. Sparse recovery with a coherent sensing matrix is important.[38,39] To achieve low coherence, Elad[40] proposes an optimized selection of the columns of $\mathbf{A}$, Gaumond and Edelmann[38] examine using a random (or optimized) array in DOA estimation, and Candés et al.[39] apply the sparsity constraint to the beamformed solution.

In the following, we provide the relevant measures of coherence of the sensing matrix $\mathbf{A}$ in DOA estimation and analyze the performance of CS in relation to this.

C. Coherence measures

An intuitive measure of correlation between any two columns of $\mathbf{A}$ is its mutual coherence defined as[3,4]

$$\mu(\mathbf{A}) = \max_{i \neq j} \mathbf{G}_{ij}, \tag{13}$$

where $\mathbf{G}_{ij}$ denotes the element in the ith row and jth column of the absolute Gram matrix,

$$\mathbf{G} = |\mathbf{A}^H \mathbf{A}|. \tag{14}$$

The elements of $\mathbf{G}$ are the inner products of the corresponding l_2-norm normalized columns of $\mathbf{A}$, Eq. (2), thus are equal to the cosine of the angle between them.

Another measure of correlation of $\mathbf{A}$ is the restricted isometry property (RIP) which is described by the restricted isometry constants.[23,24] The sth restricted isometry constant δ_s of a matrix $\mathbf{A} \in \mathbb{C}^{M \times N}$ with l_2-norm normalized columns is the smallest non-negative number such that

$$(1 - \delta_s)\|\mathbf{x}\|_2^2 \leq \|\mathbf{Ax}\|_2^2 \leq (1 + \delta_s)\|\mathbf{x}\|_2^2, \tag{15}$$

for all s-sparse vectors $\mathbf{x} \in \mathbb{C}^N$. The matrix $\mathbf{A}$ satisfies the RIP of order s if $\delta_s \in (0, 1)$. It is more informative to prove the RIP of order $2s$ since $\delta_{2s} < 1$ yields $\|\mathbf{A}(\mathbf{x} - \mathbf{x}')\|_2^2 > 0$ for every s-sparse $\mathbf{x} \neq \mathbf{x}'$, $\mathbf{x}$, $\mathbf{x}' \in \mathbb{C}^N$ assuring that distinct s-sparse signals correspond to distinct measurement vectors, $\mathbf{y} \neq \mathbf{y}'$.[4]

Let $\mathbf{A}_S$ be a submatrix composed by any set $S \subset N$ of normalized columns of $\mathbf{A}$ with cardinality card$(S) \leq s$. The condition (15) implies that the Gram matrix $\mathbf{G}_S = \mathbf{A}_S^H \mathbf{A}_S$ has its eigenvalues in the interval $[1 - \delta_s, 1 + \delta_s]$ and if $\delta_s \in (0, 1)$ then $\mathbf{G}_S$ has full rank.[24] It follows that $\delta_1 = 0$, $\delta_2 = \mu$, and, since the sequence of restricted isometry constants is nondecreasing,[4] $\delta_{s>2} \geq \mu$. Therefore, the simple measure of mutual coherence, Eq. (13), usually suffices as an indicator of coherence.

D. Coherence of the sensing matrix in DOA estimation

The sensing matrix $\mathbf{A} = [\mathbf{a}(\theta_1), ..., \mathbf{a}(\theta_N)]$ is formed by the column steering vectors on an angular grid of $i = 1, ..., N$ DOAs, $\theta_i \in [-90°, 90°]$; see Eq. (2). Hence, from Eq. (14), the columns or equivalently the rows of $\mathbf{G}$ represent the beampattern for the corresponding focusing direction (see Sec. III A).

The mutual coherence of the sensing matrix $\mathbf{A}$, i.e., the maximum off-diagonal element in $\mathbf{G}$ [see Eq. (13)], is determined by the frequency, the geometry of the array and the discretization of the angular space. To demonstrate this, we study a uniform linear array (ULA) with $\mathbf{r} = [0 : M - 1]d$ for simplicity. In this case,

$$(\mathbf{A}^H \mathbf{A})_{N \times N} = \frac{1}{M} \begin{bmatrix} M & \cdots & \sum_{q=0}^{M-1} e^{j2\pi q(d/\lambda)(\sin\theta_1 - \sin\theta_N)} \\ \sum_{q=0}^{M-1} e^{j2\pi q(d/\lambda)(\sin\theta_2 - \sin\theta_1)} & \cdots & \sum_{q=0}^{M-1} e^{j2\pi q(d/\lambda)(\sin\theta_2 - \sin\theta_N)} \\ \vdots & \vdots & \vdots \\ \sum_{q=0}^{M-1} e^{j2\pi q(d/\lambda)(\sin\theta_N - \sin\theta_1)} & \cdots & M \end{bmatrix} \tag{16}$$

hence the elements of $\mathbf{G}$ are sampled from the periodic sinc function $f(x)$,

$$f(x) = \frac{1}{M}\left|\sum_{q=0}^{M-1}e^{j2\pi q(d/\lambda)x}\right| = \frac{1}{M}\left|\frac{\sin\left(\pi M \frac{d}{\lambda}x\right)}{\sin\left(\pi\frac{d}{\lambda}x\right)}\right|, \qquad (17)$$

such that

$$\mathbf{G}_{ij} = \frac{1}{M}\left|\frac{\sin\left(\pi M \frac{d}{\lambda}\left(\sin\theta_i - \sin\theta_j\right)\right)}{\sin\left(\pi\frac{d}{\lambda}\left(\sin\theta_i - \sin\theta_j\right)\right)}\right|.$$

Figures 3(a), 3(b) and 3(c), 3(d) show the matrix $\mathbf{G}$ (i.e., the beampattern) as a function of $\sin\theta$ and θ, respectively. When the DOA grid is formed so that $\sin\theta_i = i[\lambda/(Md)]$ or, equivalently, $\theta_i = \sin^{-1}i[\lambda/(Md)]$, where $i = 0, 1, \ldots, M-1$ (*), the columns of $\mathbf{A}$ form an orthonormal system, i.e., $\mu(\mathbf{A}) = 0$. In this case, $\mathbf{A}$ is square and Fig. 3(e) shows the corresponding $\mathbf{G} = \mathbf{I}_{M=N}$.

To achieve super-resolution, a finer grid is required resulting in a nonorthonormal sensing matrix $\mathbf{A}$. Since the row and the column rank of a matrix are equal, a sensing matrix in an underdetermined problem has linearly
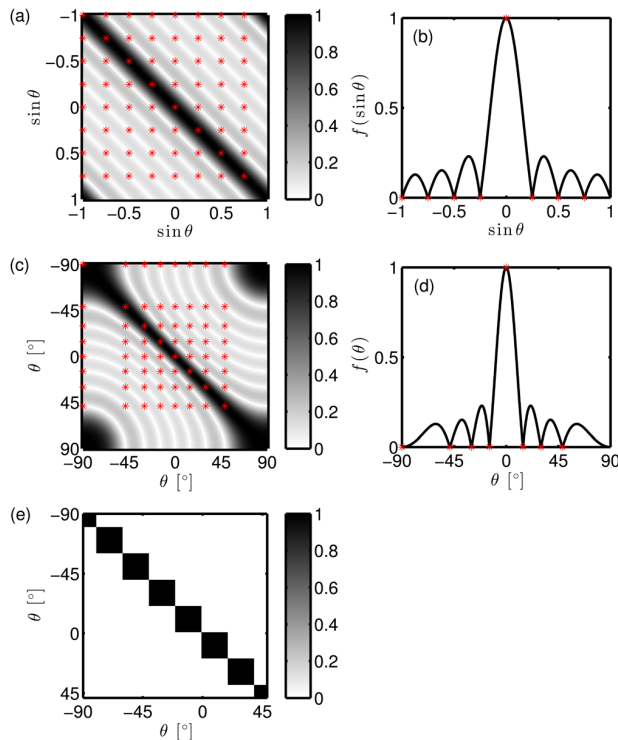

FIG. 3. (Color online) Gram matrix $\mathbf{G}$ in (a) $\sin\theta$ and (c) θ space for a ULA with $M = 8$ sensors and $d/\lambda = 1/2$. Corresponding beampattern at broadside in (b) $\sin\theta$ and (d) θ space. Discretization of the DOA grid (*) such that $\sin\theta_i = i[\lambda/(Md)]$, $i = 0, \ldots, M-1$ (a), (b) or, equivalently, $\theta_i = \sin^{-1}i[\lambda/(Md)]$, $i = 0, \ldots, M-1$ (c), (d) leads to (e) an orthonormal Gram matrix ($\mu = 0$).

dependent columns. The degree of the linear dependency of the columns of $\mathbf{A}$ is reflected in the coherence.

Figure 4 depicts the Gram matrix for an oversampled DFT (fine angular grid) for three array configurations with the same number of sensors. Grating lobes appear within the visible area when the array spacing is $d/\lambda > 1/2$, Figs. 4(b) and 4(e). A simple way to decrease the coherence of the representation while keeping the number of sensors small is to employ random arrays which lack periodicity, Figs. 4(c) and 4(f).

E. Offset and coherence

In the case of a coherent sensing matrix, uniqueness of the CS solution is not guaranteed (Sec. IV C) thus the DOA of the CS solution, $\hat{\theta}$, may be offset from the actual DOA, θ, resulting in erroneous localization, $\hat{\theta} - \theta \neq 0$. In the absence of spatial aliasing, the coherence of $\mathbf{A}$ is mostly limited to the proximity of the actual directions and it is dependent on the grid spacing relative to the aperture in terms of wavelength. Thus, the maximum CS offset, $\max|\hat{\theta} - \theta|$, is related to the beampattern and the SNR and can be predicted.

Reformulating the constraint in the optimization problem (P_1^ϵ) by denoting the true solution as $\mathbf{x}_s$,

$$\|\mathbf{Ax} - \mathbf{y}\|_2 = \|\mathbf{Ax} - (\mathbf{Ax}_s + \mathbf{n})\|_2$$
$$= \|\mathbf{A}(\mathbf{x} - \mathbf{x}_s) - \mathbf{n}\|_2 \leq \epsilon, \qquad (18)$$

and applying the reverse triangle inequality, $|\|\mathbf{u}\|_2 - \|\mathbf{v}\|_2| \leq \|\mathbf{u} - \mathbf{v}\|_2$, where $\mathbf{u}, \mathbf{v}$ are generic vectors, yields

$$|\|\mathbf{A}(\mathbf{x} - \mathbf{x}_s)\|_2 - \|\mathbf{n}\|_2| \leq \|\mathbf{A}(\mathbf{x} - \mathbf{x}_s) - \mathbf{n}\|_2 \leq \epsilon,$$
$$-\epsilon \leq \|\mathbf{A}(\mathbf{x} - \mathbf{x}_s)\|_2 - \|\mathbf{n}\|_2 \leq \epsilon,$$
$$0 \leq \|\mathbf{A}(\mathbf{x} - \mathbf{x}_s)\|_2 \leq 2\epsilon. \qquad (19)$$

Thus, all vectors $\mathbf{x}$ for which the error norm satisfies $0 \leq \|\mathbf{A}(\mathbf{x} - \mathbf{x}_s)\|_2 \leq 2\epsilon$ are possible solutions to the (P_1^ϵ) problem.

To demonstrate the relation of the CS offset to the mutual coherence of the sensing matrix (i.e., the δ_2 isometry constant; see Sec. IV C) and the SNR we assume that $\mathbf{x}_s$ and $\mathbf{x}$ each have a single nonzero element, x_s at θ_j and x at θ_i, respectively, such that $\|\mathbf{x}_s\|_0 = 1$, $\|\mathbf{x}\|_0 = 1$ which yields,

$$\|\mathbf{A}(\mathbf{x} - \mathbf{x}_s)\|_2 = \|x\mathbf{a}_i - x_s\mathbf{a}_j\|_2^2 \leq 2\epsilon, \qquad (20)$$
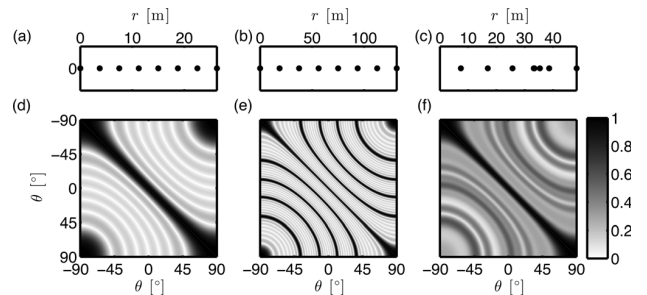

FIG. 4. Array configurations with $M = 8$ sensors at $\lambda = 7.5$ m for a ULA with (a) $d/\lambda = 1/2$, (b) $d/\lambda = 5/2$, (c) a random array. (d)–(f) The corresponding Gram matrices.

where the notation for the steering vectors is simplified such that $\mathbf{a}(\theta_i) = \mathbf{a}_i$.

The optimal value of x which minimizes the error norm $q(x) = \|x\mathbf{a}_i - x_s\mathbf{a}_j\|_2^2 = x^H x - x^H x_s \mathbf{a}_i^H \mathbf{a}_j - x_s^H x \mathbf{a}_j^H \mathbf{a}_i + x_s^H x_s$ for every θ_i, θ_j is the solution to $\partial q(x)/\partial x = 0$,

$$x = x_s \mathbf{a}_i^H \mathbf{a}_j. \tag{21}$$

Inserting the value for x from Eq. (21) into Eq. (20),

$$\|(\mathbf{a}_i^H \mathbf{a}_j)\,\mathbf{a}_i - \mathbf{a}_j\|_2 \leq 2\rho, \tag{22}$$

where $\rho = \|\mathbf{n}\|_2/\|\mathbf{A}x_s\|_2 = \epsilon/|x_s| = 10^{-\text{SNR}/20}$ is the relative noise level dictated by the SNR. Therefore, the CS DOA, θ_i, may be offset from the true, θ_j, within a region where,

$$\mathbf{G}_{ij} \geq \begin{cases} \sqrt{1 - 4\rho^2}, & \rho < \dfrac{1}{2}, \\ 0, & \rho \geq \dfrac{1}{2}. \end{cases} \tag{23}$$

In other words, the SNR sets a coherence limit, $\sqrt{1 - 4\rho^2}$, for the steering vectors, $\mathbf{a}$, below which accurate DOA reconstruction with CS is not guaranteed. For SNR lower than 6 dB ($\rho \geq \frac{1}{2}$), Eq. (23) yields $\mathbf{G}_{ij} \geq 0$, hence CS may erroneously localize the source at any angle.

Figure 5 depicts the reconstructed DOA and the estimate offset for one source for DOA 0°–90°. Figure 5(c) shows a detail from Fig. 5(b) towards endfire superimposed to the values of the error norm at the optimal x up to 2ρ, Eq. (22). Even though the CS error is determined by the specific noise realization, the offset region can be identified where $\mathbf{G}_{ij} \geq \sqrt{1 - 4\rho^2}$ and is more pronounced towards endfire where the steering vectors are more correlated.

F. Resolution and coherence

The resolution limit of a DOA estimation method is determined by the minimum required angular separation of
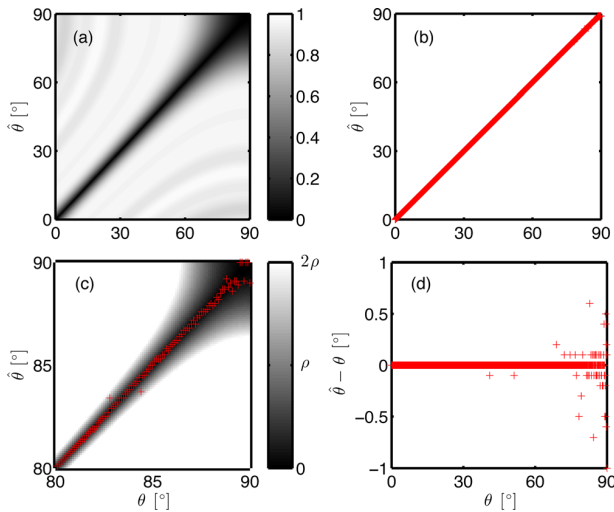

FIG. 5. (Color online) (a) Error norm $\|(\mathbf{a}_i^H \mathbf{a}_j)\,\mathbf{a}_i - \mathbf{a}_j\|_2$, Eq. (22), for the random array in Fig. 4(c), angular grid spacing 0.1° and SNR = 40 dB ($\rho = 0.01$). (b) Reconstructed DOA. (c) Detail (80°–90°) from showing the reconstructed DOA in (b) and the error norm in (a) for values up to 2ρ. (d) Offset of the CS solution for one source in relation to the actual DOA.
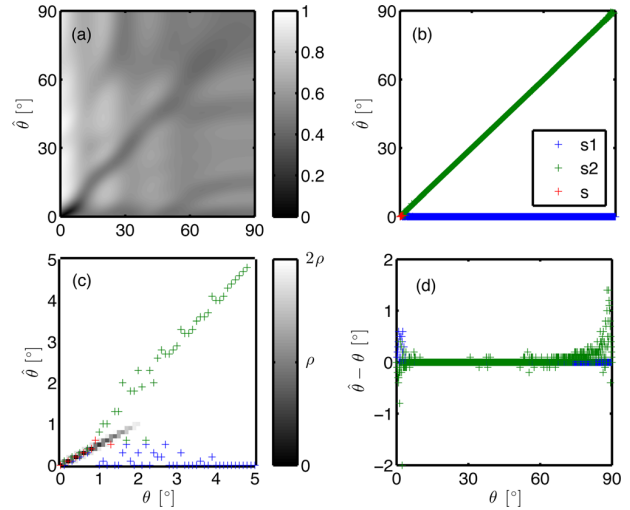

FIG. 6. (Color online) (a) Error norm $\frac{1}{2}\|\mathbf{a}_k^H(\mathbf{a}_i + \mathbf{a}_j)\mathbf{a}_k - \mathbf{a}_i - \mathbf{a}_j\|_2$, Eq. (26), for the random array in Fig. 4(c), angular grid spacing 0.1° and SNR = 40 dB ($\rho = 0.01$). (b) Reconstructed DOAs. (c) Detail (0°–5°) from showing the reconstructed DOAs in (b) and the error norm in (a) for values up to 2ρ. (d) Estimate offset for a source at 0° and a source at 0°–90°.

two sources to be resolved as separate. In this section, the CS resolution limit is discussed in relation to the coherence of the sensing matrix and the SNR.

Let the true solution, $\mathbf{x}_s$, comprise two sources at θ_i and θ_j. The two sources may not be resolved as separate by CS whenever a solution, $\mathbf{x}$, with only one source at θ_k is possible, i.e., when the error norm $0 \leq \|\mathbf{A}(\mathbf{x} - \mathbf{x}_s)\|_2 \leq 2\epsilon$ while $\|\mathbf{x}_s\|_1 = \|\mathbf{x}\|_1$.

To analyze this we let the two sources in the vector $\mathbf{x}_s$ have equal strength, $x_s/2$, the one with DOA at $\theta_i = 0°$ (Fig. 6) or $\theta_i = 90°$ (Fig. 7) and the other at θ_j moving from 0° to 90°, while the vector $\mathbf{x}$ comprises one source at θ_k with strength x, moving from 0° to 90°. Following Eq. (20),
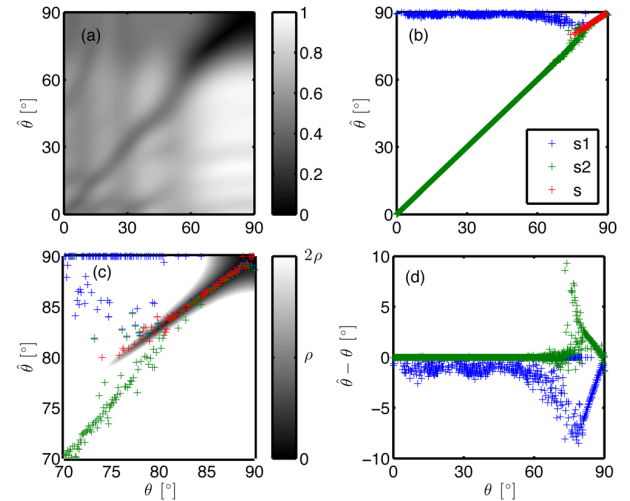

FIG. 7. (Color online) (a) Error norm $\frac{1}{2}\|\mathbf{a}_k^H(\mathbf{a}_i + \mathbf{a}_j)\mathbf{a}_k - \mathbf{a}_i - \mathbf{a}_j\|_2$, Eq. (26), for the random array in Fig. 4(c), angular grid spacing 0.1° and SNR = 40 dB ($\rho = 0.01$). (b) Reconstructed DOAs. (c) Detail (70°–90°) from showing the reconstructed DOAs in (b) and the error norm in (a) for values up to 2ρ. (d) Estimate offset for a source at 90° and a source at 0°–90°.

Xenaki *et al.*: Compressive beamforming

$$\|\mathbf{A}(\mathbf{x} - \mathbf{x}_s)\|_2^2 = \left\| x\mathbf{a}_k - \frac{x_s}{2}\mathbf{a}_i - \frac{x_s}{2}\mathbf{a}_j \right\|_2 \leq 2\epsilon. \qquad (24)$$

Similar to Eq. (21), the optimal value of the x is

$$x = x_s \frac{\mathbf{a}_k^H}{2}(\mathbf{a}_i + \mathbf{a}_j), \qquad (25)$$

and Eq. (24) yields

$$\frac{1}{2}\|\mathbf{a}_k^H(\mathbf{a}_i + \mathbf{a}_j)\mathbf{a}_k - \mathbf{a}_i - \mathbf{a}_j\|_2 \leq 2\rho. \qquad (26)$$

In contrast to Eq. (23), there is no simple expansion of Eq. (26) in terms of $\mathbf{G}$.

The resolution analysis is depicted in Figs. 6 and 7 at broadside and endfire, respectively, for the random array in Fig. 4(c). The two sources are possibly resolved as one when the angular separation of the sources is less than 2° at broadside and up to 15° at endfire.

Figure 8 shows the angular resolution limit of CS for two sources near broadside, Figs. 8(a) and 8(b), and near endfire, Figs. 8(c) and 8(d) as a function of SNR and compares it with the half-power (−3 dB) beamwidth.

V. SPARSITY AND ESTIMATED NOISE LEVEL

A basic assumption in CS is sparsity of the signal in the representation basis. In the presence of noise, the solution to (P_1) is non-sparse but still a sparse solution can be found instead by solving (P_1^ϵ) or (P_1^η) equivalently. However, when the data noise level $\|\mathbf{n}\|_2$ is unknown, the solution to both (P_1^ϵ) and (P_1^η) depends on the estimated noise level. By underestimating the noise, i.e., ϵ in (P_1^ϵ) or η in (P_1^η), the CS solution may appear as less sparse than the actual solution. On the other hand, overestimating the noise may cause the CS solution to be too sparse, for example by eliminating sources of smaller strength.
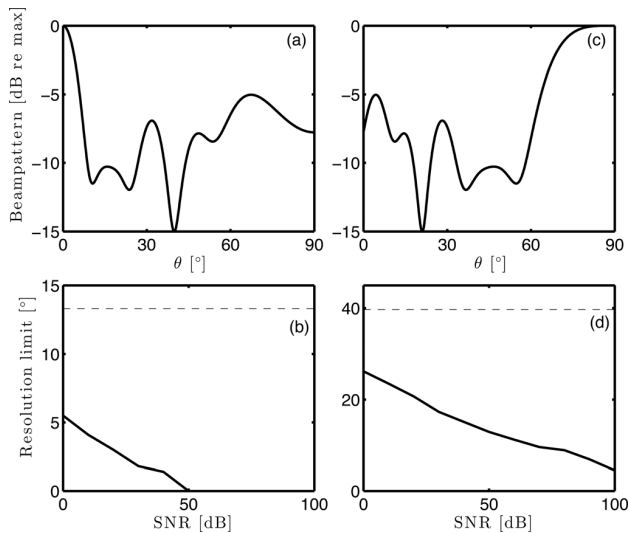

FIG. 8. CS resolution limit for two sources. Beampattern at (a) broadside and (b) endfire for the random array in Fig. 4(c). Resolution limit versus SNR at (b) broadside and (d) endfire. The half-power beamwidth (dashed line) is indicated in both cases.

In the case that the noise level is not explicitly known, we propose using an underestimated (low) noise level, to assure that all the nonzero components of the solution are captured, and enhance sparsity by reweighing the l_1-norm iteratively in the convex optimization procedure.[17,18] After detecting the source locations in the solution with reweighed l_1-norm minimization, the source amplitudes can be rectified with a level correction step.

A. Reweighed l_1 minimization

The l_1-norm minimization (P_1^ϵ) is a convex problem and converges to a global minimum. However, the solution to (P_1^ϵ) is not necessarily the sparsest feasible. To enhance sparsity, a reweighed l_1 minimization problem can be solved instead.

The method solves iteratively the weighed l_1-norm minimization problem (see the Appendix for details),

$$\min_{\mathbf{x} \in \mathbb{C}^n} \|\mathbf{W}\mathbf{x}\|_1 \text{ subject to } \|\mathbf{A}\mathbf{x} - \mathbf{y}\|_2 \leq \epsilon, \qquad (P_1^w)$$

where $\mathbf{W}$ is a diagonal weight matrix. Initially, all the weights are 1 leading to the problem (P_1^ϵ). After the first estimate $\mathbf{x}$, the weights are updated as

$$w_i = \frac{1}{|\hat{x}_i| + \xi} \qquad (27)$$

and the problem (P_1^w) is solved again. The parameter $\xi > 0$ ensures that a null coefficient in the current estimate does not suppress a nonzero coefficient in the next iteration. It should be on the order of the smallest expected source amplitude. The algorithm iterates until a stable estimate is reached, i.e., $\hat{\mathbf{x}}^{k+1} = \hat{\mathbf{x}}^k$, where

$$|w_i x_i|^{k+1} = \begin{cases} \dfrac{|x_i|}{|x_i| + \xi} \approx 1, & |x_i| > 0, \\ 0, & x_i = 0, \end{cases} \qquad (28)$$

thus it has converged (usually one or two iterations suffice).

The weights in Eq. (27) are large for small coefficients, $|x_i|$, and vice versa. Therefore, the smaller coefficients, as indicated by the current solution, are amplified by the weighing, Eq. (27), thus are penalized more in the minimization (P_1^w).

Figure 9 shows the process of reweighing the l_1-norm minimization problem. The solution to (P_1^ϵ) with $\epsilon = 0.8\|\mathbf{n}\|_2$, Fig. 9(a), appears less sparse than the actual solution due to the lower noise level. Overestimating the noise level, Fig. 9(b), erroneously favors very sparse solutions suppressing the weakest source in the estimated solution. Figures 9(c) and 9(d) show the solution to (P_1^w) with $\epsilon = 0.8\|\mathbf{n}\|_2$ after the first and second iteration, respectively. Reweighing the l_1-norm results in a more sparse solution compared to (P_1^ϵ) even though the noise level is underestimated. The (P_1^w) leads to the actual solution already from the first iteration thus the computational burden is not increased significantly compared to (P_1^ϵ).

B. Level correction

The sparse solution to (P_1^w) can be further improved with level correction. Retaining only the columns in $\mathbf{A}$ which
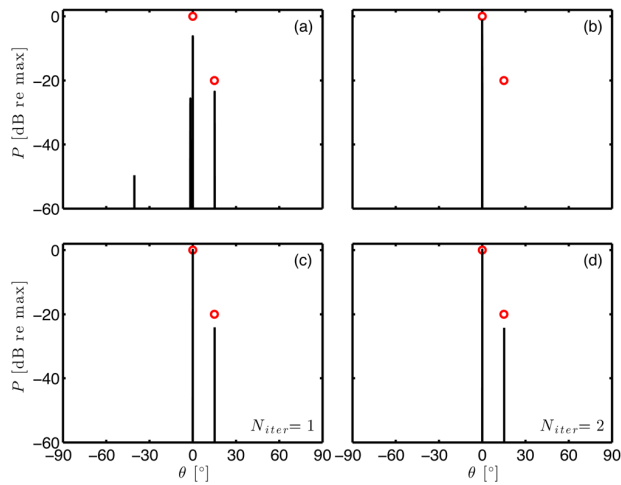
FIG. 9. (Color online) Enhancing sparsity by reweighted l_1 minimization. Two sources at $[0°,15°]$ with SNR $[20,0]$ dB, respectively, are detected by measurements on the random linear array in Fig. 4(c). The solution to the (P_1^ϵ) with (a) underestimated noise level $\epsilon = 0.8\|\mathbf{n}\|_2$, (b) overestimated noise level $\epsilon = 2\|\mathbf{n}\|_2$, and the solution to the (P_1^w) with $\epsilon = 0.8\|\mathbf{n}\|_2$ after the (c) first and (d) second iteration.

correspond to peaks in the solution, $\mathbf{A}_a$, we solve the overdetermined problem,[35,41]

$$\hat{\mathbf{x}}_a = \mathbf{A}_a^+ \mathbf{y}, \tag{29}$$

where the plus sign denotes pseudo-inverse of a matrix, to obtain the source level for just the active indexes.

Figure 10 compares the solutions from CBF, CS, reweighed CS and reweighed CS with level correction. CBF fails to detect the weakest source due to the high sidelobe levels even though the separation of the two sources exceeds half of the mainlobe width. The two sources are localized with high resolution with CS and the estimate is more accurate with reweighed CS. Further processing for level correction gives very good reconstruction.

VI. EXPERIMENTAL RESULTS

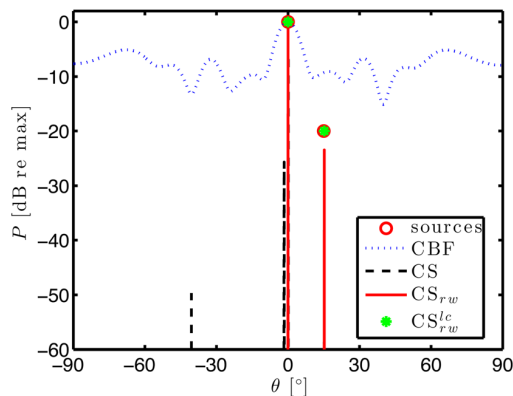To demonstrate the high-resolution capabilities and the robustness of CS in DOA estimation, the method is applied

FIG. 10. (Color online) DOA estimation with CBF, CS, reweighed CS and reweighed CS with level correction with the random linear array in Fig. 4(c), for two sources at $[0°,15°]$ and SNR $[20,0]$ dB, respectively.

to ocean acoustic measurements for source tracking from single snapshot data and is compared with CBF. More elaborate techniques, such as, for example, multi-rate adaptive beamforming[42] or post-processing with the method of subband peak energy detection,[43] would provide cleaner reconstruction than CBF by exploiting information from several snapshots. The main interest is to show the performance of CS as a non-adaptive technique and in challenging scenarios of few snapshots (or even a single one) thus we compare CS simply with CBF.

The data are from the long range acoustic communications (LRAC) experiment[44] collected from a towed horizontal uniform linear array from 10:00–10:30 UTC on 16 September 2010 in the NE Pacific. The array has $M = 64$ sensors, with intersensor spacing $d = 3\,\mathrm{m}$, Fig. 11(a), and was towed at 3.5 knots at 200 m depth. The data were acquired with a sampling frequency of 2000 Hz and the record is divided in 4 s non-overlapping snapshots. Each snapshot is Fourier transformed with 2^{13} samples.

Figure 11(b) shows the scaled Gram matrix $\mathbf{G}$ at frequency $f = 125\,\mathrm{Hz}$ $(d/\lambda = 1/4)$ for a DOA grid $[-90°:1°:90°]$. The 1° grid spacing is considered sufficient to avoid basis mismatch in this case since a finer grid would not improve the results. The data are post-processed with CBF, CS, and iterative reweighed CS with level correction
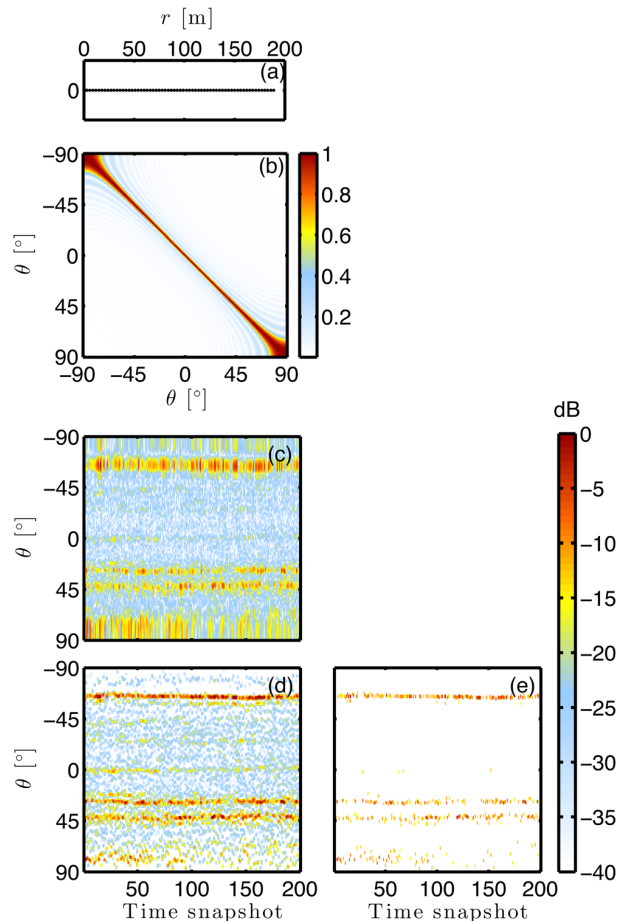

FIG. 11. (Color online) Data from LRAC: (a) Array geometry, (b) Gram matrix $\mathbf{G}$, (c) CBF, (d) CS, (e) reweighed CS with level correction.
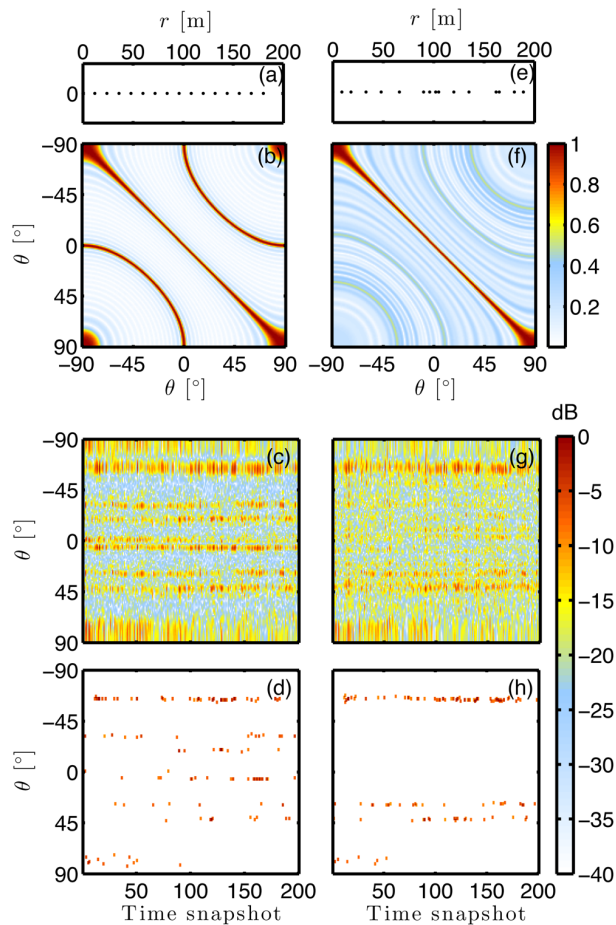
FIG. 12. (Color online) Data from LRAC: (a)–(d) $M = 16$ arranged in a ULA, (e)–(h) $M = 16$ arranged in a random linear array. (a),(e) Array configurations; (b),(d) corresponding Gram matrix; (c),(g) CBF; (d),(h) reweighed CS with level correction.

FIG. 13. (Color online) Data from LRAC: Combining the 200 snapshots and processing with CBF, MVDR, MUSIC, and reweighed CS with level correction. The ULA array with $M = 64$ sensors and $d/\lambda = 1/4$ is used.

in Figs. 11(c)–11(e). The unconstrained (P_1^η) formulation of CS is used here with $\eta = 1$.

The beamformer output, Fig. 11(c), indicates the presence of three stationary sources at around 45°, 30°, and −65°. The two arrivals at 45° and 30° are attributed to distant transiting ships, even though a record of ships in the area was not kept. The broad arrival at −65° is from the tow-ship R/V Melville. The CBF map suffers from low resolution and artifacts due to sidelobes and noise. The CS map provides high resolution, Fig. 11(d). The reconstruction is further improved with one iteration of reweighed CS with level correction, Fig. 11(e), which eliminates the noisy artifacts.

The same data set is processed by reducing the sensors by a factor of 4 to $M = 16$ for a ULA with $d/\lambda = 1$, Figs. 12(a)–12(d), and a random array, Figs. 12(e)–12(h). Both array configurations, Figs. 12(a) and 12(e), have the same aperture as the original array hence the same resolution. In the case of the ULA with $d/\lambda = 1$, grating lobes appear in the visible area, Fig. 12(b), resulting in spurious sources in both CBF, Fig. 12(c), and CS, Fig. 12(d). In the case that the sensors are selected randomly, there are no grating lobes in the beampattern, Fig. 12(f), thus spurious sources do not appear. The increased level of sidelobes in this case degrades the CBF map, Fig. 12(g). In contrast, CS, Fig. 12(h), results in a clean map with accurate localization of
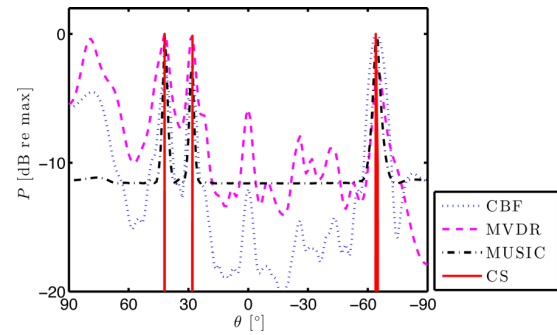
the three sources. The robustness of CS even with a limited number of sensors indicates the possibility of using arrays with fewer sensors (reducing the cost, exceeding the design frequency) without a significant reconstruction degradation as long as the configuration is random.

Assuming the sources are adequately stationary, the 200 snapshots are combined to compare the CS method with CBF, MVDR, and MUSIC (see Sec. III). The superior performance of CS in terms of resolution and sidelobe levels is depicted in Fig. 13.

VII. CONCLUSION

Source localization with sensor arrays is a sparse signal reconstruction problem which can be efficiently solved with compressive sensing (CS). The offset and resolution analysis indicates that the CS has robust performance in most of the angular spectrum. The CS estimate offset in DOA estimation is related to the coherence of the sensing matrix $\mathbf{A}$ and is restricted to the proximity of the actual source location. Similarly, the resolution of CS is determined by the coherence of $\mathbf{A}$ and depends on array geometry, frequency, source location, and SNR.

CS achieves high-resolution in DOA estimation by promoting sparse solutions. It can distinguish between coherent arrivals, as multipath, since it does not involve the array cross-spectral matrix and can be used even with single-snapshot data outperforming traditional DOA estimation methods. Furthermore, CS can be used with (arbitrary) random array configurations allowing great flexibility in the context of sound source localization.

ACKNOWLEDGMENT

APPENDIX: REWEIGHED l_1 MINIMIZATION

To enhance sparsity, the l_1-norm of a vector, $\mathbf{x} \in \mathbb{C}^N$, can be replaced by other sparsity promoting functions such as, $J(\mathbf{x}) = \sum_{i=1}^{N} \ln(|x_i| + \xi)$, resulting in the optimization problem,

$$\min_{\mathbf{x} \in \mathbb{C}^N} J(\mathbf{x}) \text{ subject to } \|\mathbf{A}\mathbf{x} - \mathbf{y}\|_2 \leq \epsilon, \qquad (P_J^\epsilon)$$

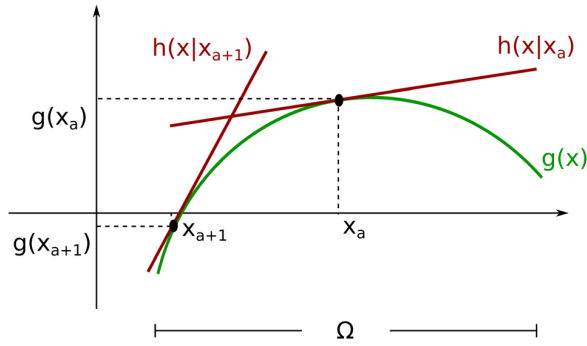instead of the problem (P_1^ϵ).

FIG. 14. (Color online) Schematic showing the majorization-minimization procedure for minimizing a concave function.

However, the function $J(\mathbf{x})$ is concave and its minimization is achieved by a majorization-minimization approach[45] rather than a convex minimization as with the l_1-norm (P_1^ϵ).

In principle, minimizing a concave function $g(\mathbf{x})$, $\mathbf{x} \in \Omega$, with the majorization-minimization framework involves the following steps (see Fig. 14):

(1) Majorize $g(\mathbf{x})$ at $\mathbf{x}_a$ with a convex function $h(\mathbf{x}|\mathbf{x}_a)$ such that for $\mathbf{x} \in \Omega$,

$$h(\mathbf{x}_a|\mathbf{x}_a) = g(\mathbf{x}_a),$$
$$h(\mathbf{x}|\mathbf{x}_a) \geq g(\mathbf{x}). \tag{A1}$$

(2) Minimize the convex function $h(\mathbf{x}|\mathbf{x}_a)$ with respect to $\mathbf{x} \in \Omega$,

$$h(\mathbf{x}_{a+1}|\mathbf{x}_a) = \min_{\mathbf{x} \in \Omega} h(\mathbf{x}|\mathbf{x}_a), \tag{A2}$$

which also assures a descent for the concave function $g(\mathbf{x})$ as

$$g(\mathbf{x}_{a+1}) \leq h(\mathbf{x}_{a+1}|\mathbf{x}_a) \leq h(\mathbf{x}_a|\mathbf{x}_a) = g(\mathbf{x}_a). \tag{A3}$$

(3) Replace steps (1) and (2) until convergence.

For a differentiable concave function $g(\mathbf{x})$, $\mathbf{x} \in \Omega$, a majorization function can be found easily by definition through the derivative

$$g(\mathbf{x}) \leq g(\mathbf{x}_a) + \nabla g(\mathbf{x}|\mathbf{x}_a)(\mathbf{x} - \mathbf{x}_a), \tag{A4}$$

and minimized such that

$$h(\mathbf{x}_{a+1}|\mathbf{x}_a) = \min_{\mathbf{x} \in \Omega} h(\mathbf{x}|\mathbf{x}_a) = \min_{\mathbf{x} \in \Omega} \nabla g(\mathbf{x}|\mathbf{x}_a)\mathbf{x}. \tag{A5}$$

Therefore, the minimization problem (P_J^ϵ) can be recast in an iterative convex optimization procedure, such that at the $(k+1)$ iteration,

$$\min_{\mathbf{x} \in \mathbb{C}^N} \nabla J(\mathbf{x}|\hat{\mathbf{x}}_k)\mathbf{x} \text{ subject to } \|\mathbf{Ax} - \mathbf{y}\|_2 \leq \epsilon,$$

$$\min_{\mathbf{x} \in \mathbb{C}^N} \sum_{i=1}^{N} \frac{1}{|\hat{x}_{i,k}| + \xi} |x_i| \text{ subject to } \|\mathbf{Ax} - \mathbf{y}\|_2 \leq \epsilon, \tag{A6}$$

where $\hat{\mathbf{x}}_k$ is the estimated solution at iteration k. The minimization problem (P_J^ϵ) is equivalent to the iterative weighed l_1-norm minimization problem (P_1^w),

$$\min_{\mathbf{x} \in \mathbb{C}^n} \|\mathbf{Wx}\|_1 \text{ subject to } \|\mathbf{Ax} - \mathbf{y}\|_2 \leq \epsilon, \tag{P_1^w}$$

where $\mathbf{W}$ is a diagonal weight matrix with elements $w_i = 1/|\hat{x}_i| + \xi$ determined by the solution of the previous iteration $\hat{\mathbf{x}}$. The weight matrix, $\mathbf{W}$, is initialized with the identity matrix, $\mathbf{I}_N$, and the parameter $\xi > 0$ is used to prevent infinite-valued weights.

[1] D. H. Johnson and D. E. Dudgeon, *Array Signal Processing: Concepts and Techniques* (PRT Prentice Hall, Englewood Cliffs, NJ, 1993), pp. 1–512.
[2] H. Krim and M. Viberg, "Two decades of array signal processing research: the parametric approach," IEEE Signal Process. Mag. **13**, 67–94 (1996).
[3] M. Elad, *Sparse and Redundant Representations: From Theory to Applications in Signal and Image Processing* (Springer, New York, 2010), pp. 1–359.
[4] S. Foucart and H. Rauhut, *A Mathematical Introduction to Compressive Sensing* (Springer, New York, 2013), pp. 1–589.
[5] E. J. Candés, J. Romberg, and T. Tao, "Robust uncertainty principles: Exact signal reconstruction from highly incomplete frequency information," IEEE Trans. Inf. Theory **52**, 489–509 (2006).
[6] M. Lustig, D. Donoho, and J. M. Pauly, "Sparse MRI: The application of compressed sensing for rapid MR imaging," Magn. Reson. Med. **58**, 1182–1195 (2007).
[7] N. Wagner, Y. C. Eldar, and Z. Friedman, "Compressed beamforming in ultrasound imaging," IEEE Trans. Signal Process. **60**, 4643–4657 (2012).
[8] E. J. Candés and T. Tao, "Decoding by linear programming," IEEE Trans. Inf. Theory **51**, 4203–4215 (2005).
[9] M. A. Herman and T. Strohmer, "High-resolution radar via compressed sensing," IEEE Trans. Signal Process. **57**, 2275–2284 (2009).
[10] H. Yao, P. Gerstoft, P. M. Shearer, and C. Mecklenbräuker, "Compressive sensing of the Tohoku-Oki Mw 9.0 earthquake: Frequency-dependent rupture modes," Geophys. Res. Lett. **38**, 1–5, doi:10.1029/2011GL049223 (2011).
[11] H. Yao, P. M. Shearer, and P. Gerstoft, "Compressive sensing of frequency-dependent seismic radiation from subduction zone megathrust ruptures," Proc. Natl. Acad. Sci. U.S.A. **110**, 4512–4517 (2013).
[12] J. Romberg, "Imaging via compressive sampling," IEEE Signal Process. Mag. **25**, 14–20 (2008).
[13] W. Mantzel, J. Romberg, and K. Sabra, "Compressive matched-field processing," J. Acoust. Soc. Am. **132**, 90–102 (2012).
[14] C. Yardim, P. Gerstoft, W. S. Hodgkiss, and J. Traer, "Compressive geoacoustic inversion using ambient noise," J. Acoust. Soc. Am. **135**, 1245–1255 (2014).
[15] D. Malioutov, M. Çetin, and A. S. Willsky, "A sparse signal reconstruction perspective for source localization with sensor arrays," IEEE Trans. Signal Process. **53**, 3010–3022 (2005).
[16] G. F. Edelmann and C. F. Gaumond, "Beamforming using compressive sensing," J. Acoust. Soc. Am. **130**, EL232–EL237 (2011).
[17] I. F. Gorodnitsky and B. D. Rao, "Sparse signal reconstruction from limited data using FOCUSS: A re-weighted minimum norm algorithm," IEEE Trans. Signal Process. **45**, 600–616 (1997).
[18] E. J. Candés, M. B. Wakin, and S. Boyd, "Enhancing sparsity by reweighted l_1 minimization," J. Fourier Anal. Appl. **14**, 877–905 (2008).
[19] T. Yardibi, J. Li, P. Stoica, M. Xue, and A. B. Baggeroer, "Source localization and sensing: A nonparametric iterative adaptive approach based on weighted least squares," IEEE Trans. Aerosp. Electron. Syst. **46**, 425–443 (2010).
[20] D. L. Donoho, "Compressed sensing," IEEE Trans. Inf. Theory **52**, 1289–1306 (2006).
[21] E. J. Candes and M. B. Wakin, "An introduction to compressive sampling," IEEE Signal Proc. Mag. **25**, 21–30 (2008).
[22] R. G. Baraniuk, "Compressive sensing," IEEE Signal Proc. Mag. **24**, 118–121 (2007).
[23] E. J. Candes, "The restricted isometry property and its implications for compressed sensing," C. R. Math. Acad. Sci. **346**, 589–592 (2008).
[24] R. G. Baraniuk, M. Davenport, R. DeVore, and M. Wakin, "A simple proof of the restricted isometry property for random matrices," Constr. Approx. **28**, 253–263 (2008).

[25] E. J. Candés and T. Tao, "Near-optimal signal recovery from random projections: Universal encoding strategies?," IEEE Trans. Inf. Theory **52**, 5406–5425 (2006).

[26] S. S. Chen, D. L. Donoho, and M. A. Saunders, "Atomic decomposition by basis pursuit," SIAM J. Sci. Comput. **20**, 33–61 (1998).

[27] S. F. Cotter, B. D. Rao, K. Engan, and K. Kreutz-Delgado, "Sparse solutions to linear inverse problems with multiple measurement vectors," IEEE Trans. Signal Process. **53**, 2477–2488 (2005).

[28] J. A. Tropp, "Just relax: Convex programming methods for identifying sparse signals in noise," IEEE Trans. Inf. Theory **52**, 1030–1051 (2006).

[29] M. Grant and S. Boyd, "CVX: Matlab software for disciplined convex programming, version 2.0 beta," http://cvxr.com/cvx (Last viewed February 3, 2013).

[30] M. Grant and S. Boyd, "Graph implementations for nonsmooth convex programs," in *Recent Advances in Learning and Control, Lecture Notes in Control and Information Sciences*, edited by V. Blondel, S. Boyd, and H. Kimura (Springer-Verlag, London, 2008), pp. 95–110.

[31] S. Boyd and L. Vandenberghe, *Convex Optimization* (Cambridge University Press, New York, 2004), pp. 1–684.

[32] H. Van Trees, *Optimum Array Processing (Detection, Estimation, and Modulation Theory, Part IV)* (Wiley-Interscience, New York, 2002), Chaps. 1–10.

[33] J. Capon, "High-resolution frequency-wavenumber spectrum analysis," Proc. IEEE **57**, 1408–1418 (1969).

[34] R. Schmidt, "Multiple emitter location and signal parameter estimation," IEEE Trans. Antennas Propag. **34**, 276–280 (1986).

[35] C. F. Mecklenbräuker, P. Gerstoft, A. Panahi, and M. Viberg, "Sequential Bayesian sparse signal reconstruction using array data," IEEE Trans. Signal Process. **61**, 6344–6354 (2013).

[36] Y. Chi, L. L. Scharf, A. Pezeshki, and A. R. Calderbank, "Sensitivity to basis mismatch in compressed sensing," IEEE Trans. Signal Process. **59**, 2182–2195 (2011).

[37] H. Monajemi, S. Jafarpour, M. Gavish, Stat 330/CME 362 Collaboration, and D. L. Donoho, "Deterministic matrices matching the compressed sensing phase transitions of Gaussian random matrices," Proc. Natl. Acad. Sci. U.S.A. **110**, 1181–1186 (2013).

[38] C. F. Gaumond and G. F. Edelmann, "Sparse array design using statistical restricted isometry property," J. Acoust. Soc. Am. **134**, EL191–EL197 (2013).

[39] E. J. Candes, Y. C. Eldar, D. Needell, and P. Randall, "Compressed sensing with coherent and redundant dictionaries," Appl. Comput. Harmon. Anal. **31**, 59–73 (2011).

[40] M. Elad, "Optimized projections for compressed sensing," IEEE Trans. Signal Process. **55**, 5695–5702 (2007).

[41] S. J. Wright, R. D. Nowak, and M. A. T. Figueiredo, "Sparse reconstruction by separable approximation," IEEE Trans. Signal Process. **57**, 2479–2493 (2009).

[42] H. Cox, "Multi-rate adaptive beamforming (MRABF)," in *Sensor Array and Multichannel Signal Processing Workshop* (IEEE, Cambridge, MA, 2000), pp. 306–309.

[43] M. Bono, B. Shapo, P. McCarty, and R. Bethel, "Subband energy detection in passive array processing," DTIC Document, Texas University–Austin Applied Research Labs (2000).

[44] H. C. Song, S. Cho, T. Kang, W. S. Hodgkiss, and J. R. Preston, "Long-range acoustic communication in deep water using a towed array," J. Acoust. Soc. Am. **129**, EL71–EL75 (2011).

[45] D. R. Hunter and K. Lange, "A tutorial on MM algorithms," Am. Stat. **58**, 30–37 (2004).